

Article

# Shading by Overhang PV Collectors

Joseph Appelbaum \* , Avi Aronescu and Tamir Maor

Tel Aviv University School of Electrical Engineering, Tel Aviv 69978, Israel; aviarone@gmail.com (A.A.); maorxtm@gmail.com (T.M.)

\* Correspondence: appel@eng.tau.ac.il

Received: 1 August 2019; Accepted: 30 September 2019; Published: 12 October 2019



**Abstract:** Photovoltaic modules integrated into buildings may provide shading to windows, doors and walls to protect against sun rays and at the same time generate ancillary electrical energy. The study develops the methodology for calculating the shadow variation cast by overhangs on doors, windows, carports, and calculates the annual incident energy (beam, diffuse and global energy) on overhangs made up of conventional and bifacial PV modules. The methodology of the present study is different from published articles including software programs. The study starts with shadows on walls cast by a horizontal pole and follows by shadows on walls cast by horizontal plates, inclined pole, inclined plate, and shaded area. The study deals also with overhangs placed one above the other. The calculation of the diffuse radiation involves the calculation of view factors to sky, to ground and between overhangs. In addition, the present study suggests using bifacial PV modules for overhangs and calculates the contribution of the reflective energy (5% and more) from walls and ground to the rear side of the bifacial PV module.

**Keywords:** BIPV; window shadowing; overhang PV collectors; bifacial PV collectors

## 1. Introduction

Photovoltaic modules are often integrated into the building envelope and may provide shading, and at the same time perform as an ancillary source of electrical power. Building-integrated photovoltaics (BIPV) are photovoltaic materials used for many years as replacements for conventional building material in some parts of the building such as roofs, canopies, facades, solar carports and others. Overhangs on south-facing walls in northern latitudes are protruding structures and are important in shading windows and doors from undesired solar heat by blocking the sunlight during the summer months. References that illustrate the concept of BIPV are mentioned in [1–9] to name only a few. There are many tools available for shading analysis and designing overhang shading structures (Solar Pathfinder, SunEye, Pilkington, Autodesk ECOTECH, METEONORM, Shadow Analyser, Sombrero, EnergyPlus, ESP-r, and many more). EnergyPlus is a building energy simulation program to model energy consumption and water use in buildings. ESP-r is a program that simulates the energy and environmental performance of buildings. Commercial ray tracing software programs are available and may be used for shading analysis (3Delight, Anim8or, ASAP). Not many publications deal with analytical expressions of the shadow variation on windows, walls and on grounds cast by overhang structures [10–15]. The methodology of the present study is different to in the above-mentioned articles including software programs. The study develops basic mathematical expressions, step by step, for calculating the shadow variation cast by overhangs on windows, carports, and for calculating the annual incident energy on overhangs made up of conventional and bifacial PV modules. The calculation of the diffuse radiation involves the calculation of view factors to sky, to ground and between overhangs. The study starts with the shadow on a wall cast by a horizontal pole and follows by shadows on a wall cast by a horizontal plate, inclined pole, inclined plate, shaded areas and overhangs placed one

above the other (see Figure 1). The present study provides an insight and methodology for calculating shadows and incident radiation on PV modules deployed on overhangs in BIPV.

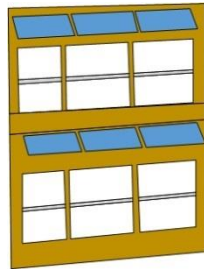


Figure 1. Overhang photovoltaic (PV) collector (blue) on building façade.

## 2. Materials and Methods

The variation of shadows on vertical objects (walls, windows, doors, etc.) is important information for designing shading elements to block solar heat in buildings. The following analysis starts with shadows cast by poles and extends to plates.

### 2.1. Shadow on a South Facing Walls Cast by a Horizontal Pole

A horizontal pole *bc* of length *H* attached perpendicular to a wall, is shown in Figure 2. The right edge “*c*” casts a shadow on the wall by the solar rays at point “*a*”.

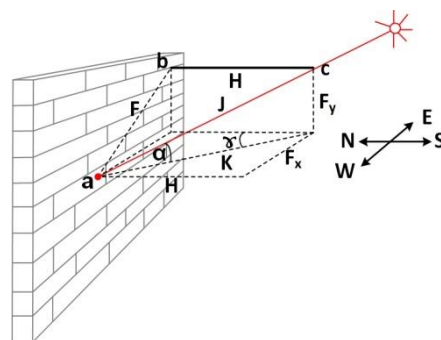


Figure 2. Horizontal pole attached perpendicular to a wall.

From Figure 2 it follows:

$$F_x = K \sin \gamma, \quad F_y = J \sin \alpha \tag{1}$$

$$J = K / \cos \alpha, \quad H = K \cos \gamma \tag{2}$$

By substituting Equation (2) into Equation (1), we get the coordinates of the shadow point “*a*”, i.e., the shadow variation on the wall during the day maybe calculated:

$$F_x = H \tan \gamma \tag{3}$$

$$F_y = H \tan \alpha / \cos \gamma \tag{4}$$

where

$$\sin \alpha = \sin \phi \sin \delta + \cos \phi \cos \delta \cos \omega \tag{5}$$

$$\cot \gamma = [\sin \phi \cos \omega - \cos \phi \tan \delta] / \sin \omega \tag{6}$$

and

$$\omega = 15T - 180 \tag{7}$$

$\alpha$  is the sun elevation angle,  $\gamma$  is the sun azimuth angle with respect to south,  $\omega$  is the solar angle ( $\omega = 0$  noon,  $\omega < 0$  morning and  $\omega > 0$  afternoon) and  $T$  is the solar time. The solar inclination angle  $\delta$  is given by:

$$\delta = 23.45 \sin \frac{(284 + n)}{365} \tag{8}$$

Figure 3 shows the shadow component,  $F_x$  and  $F_y$ , of a pole attached perpendicular to a wall at the origin 0,0,0 calculated according Equations (3)–(8) for Tel Aviv (latitude  $\phi = 32^\circ N$ ) for the months December to April on 21st day. The arrows indicate the shadow length at given hours before noon. On vernal equinox ( $\delta = 0^\circ$ ) the  $F_y$  component is constant during the day. In afternoon hours, the shadow is symmetrical with respect to the Y axis.

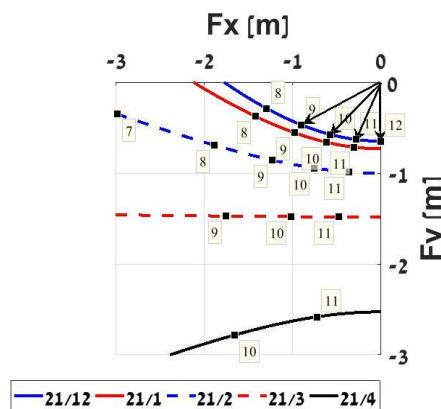


Figure 3. Shadow trajectory by horizontal pole on a wall, December to April on 21st day.

### 2.2. Shadow on Walls Cast by Horizontal Plate

A horizontal plate  $bcd$  of length  $L$  and width  $H$ , attached perpendicular to a wall on side  $\overline{bd}$  located above a window (not shown), is shown in Figure 4. The trajectory of the shadow on the window is shown in Figure 5 on 21st January before noon (blue lines) and at 12:00 noon (dashed lines). A plate may be considered as composed of an infinite number of poles; therefore Equations (3)–(8) are applied to obtain the shadow trajectory on the window. At 08:00 the shadow takes the form of a parallelogram (blue) and at noon time the shadow is rectangular (yellow).

Now we extend the calculation of a shadow on a wall for the case where the plate is inclined with an angle  $\epsilon$  downwards, see Figure 6.

From Figure 6 we write:

$$H = A \sin \epsilon, \quad P_y = F_y + A \cos \epsilon$$

and by substituting in Equation (4) we calculate the coordinates of point “a”, i.e.,  $P_x$  (see Equation (3)) and  $P_y$ :

$$P_x = A \sin \epsilon \tan \gamma \tag{9}$$

$$P_y = (A \sin \epsilon \tan \alpha / \cos \gamma) + A \cos \epsilon \tag{10}$$

The shadow variation (Equations (9), (10)) on the wall during the day may now be obtained similarly to the procedure for the horizontal plate.

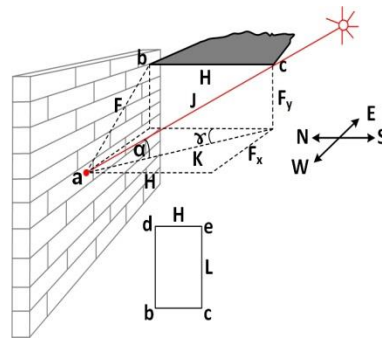


Figure 4. Horizontal plate attached perpendicular to a wall.

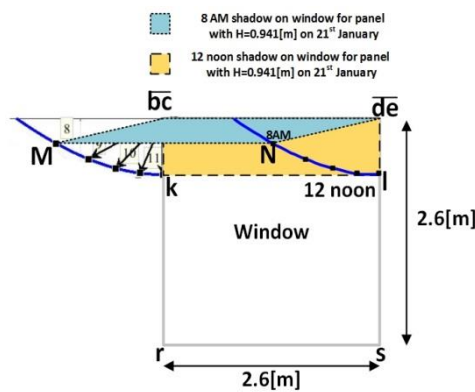


Figure 5. Shadow variation on a window on 21st January (blue lines) and at 12:00 noon (dashed lines).

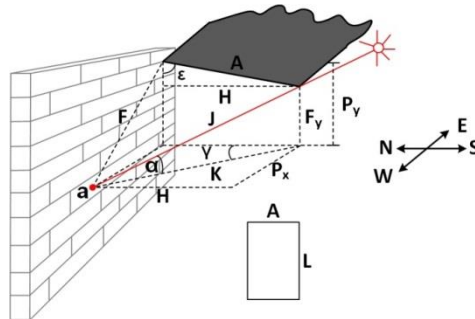


Figure 6. Inclined plate attached to a wall.

### 2.3. Shadow of a Horizontal Pole on a Horizontal Plate

A horizontal pole  $bc$  of length  $H$  attached perpendicular to a wall at point  $b$  (origin  $0,0,0$ ), is shown in Figure 7. The plate is located at a distance  $R$  under the pole. The right edge "c" of the pole casts a shadow at point  $F$  on the plate, and point "d" cast a shadow at point  $E$ , i.e., the length  $dc$  of the pole cast the shadow  $EF$  on the plate at a right angle to the wall. The length  $bd$  of the pole cast a shadow  $bE$  on the wall. The shadow length  $EF$  is given by (see Appendix A in [16]):

$$EF = Z_F = H(1 - R/F_y) \tag{11}$$

and the distance  $OE$  is:

$$OE = X_F = RF_x/F_y \tag{12}$$

where  $F_x$  and  $F_y$  is given in Equations (3) and (4), respectively.

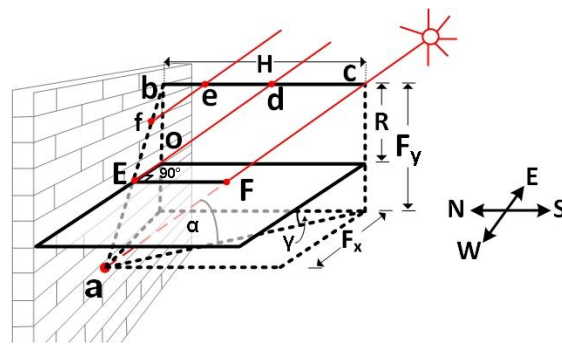


Figure 7. Shadow of a horizontal pole on a horizontal plate.

Figure 8 shows the shadow component,  $EF$  and  $OE$ , of a pole  $H = 0.941m$  attached perpendicular to a wall at a distance  $R = 3.0m$  above a horizontal plate, calculated according to Equations (11)–(12) for Tel Aviv (latitude  $\phi = 32^\circ N$ ) for the months May, June and July on the 21st day. The arrows indicate the shadow length at given hours before noon.

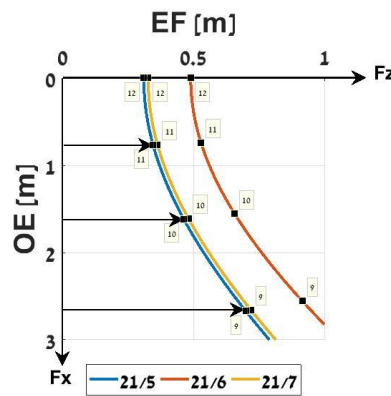


Figure 8. Shadow trajectory of a horizontal pole on a horizontal plate.

#### 2.4. Shadow of an Inclined Pole on a Horizontal Plate

Proceeding with our analysis, we develop now the expression for a shadow cast on a horizontal plate by an inclined pole of length  $A$  attached downwards to a wall with an angle  $\varepsilon$  with respect to the wall, see Figure 9. Based on Appendix A in [16] and after some mathematical manipulation one obtains the coordinates of points  $F$  and  $E$ , respectively:

$$X_F = \frac{P_x(R - A \cos \varepsilon)}{P_y - A \cos \varepsilon} \quad (13)$$

$$Y_F = R \quad (14)$$

$$Z_F = \frac{A \sin \varepsilon (P_y - R)}{P_y - A \cos \varepsilon} \quad (15)$$

$$X_E = RP_x/P_y \quad (16)$$

$$Y_E = R \quad (17)$$

$$Z_E = 0 \quad (18)$$

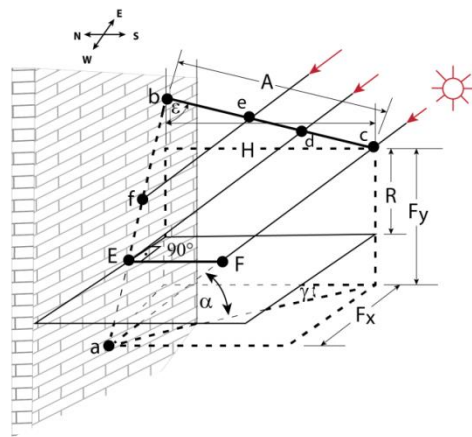


Figure 9. Shadow of an inclined pole on a horizontal plate.

2.5. Shadow by Inclined Plates

We now analyze the mutual shading by two parallel plates, one above the other, attached to a wall and inclined with an angle  $\epsilon$  downwards. The length and width of the plates are  $L$  and  $A$ , respectively, as shown in Figure 10.

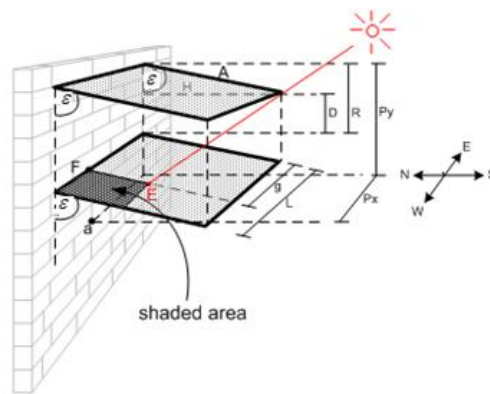


Figure 10. Inclined plates one above another.

Based on Appendix A in [16], the length of segments  $\bar{g}$  and  $\overline{EF}$  are given by:

$$\bar{g} = (R \times P_x) / P_y \tag{19}$$

$$\overline{EF} = A(1 - R/P_y) \tag{20}$$

$$R = A \cos \epsilon + D \tag{21}$$

The shaded area is given by:

$$\overline{EF} \times (L - \bar{g}) \tag{22}$$

and the relative shaded area  $S^{sh}$  is given by:

$$S^{sh} = \frac{EF}{A} \cdot \frac{(L - \bar{g})}{L} = \left(1 - \frac{R}{P_y}\right) \cdot \left(1 - \frac{P_x \cdot R}{P_y \cdot L}\right) \tag{23}$$

For the case of horizontal plates ( $\epsilon = 90^\circ$ ) we have (see Equation (21)  $R = D$ ,  $\bar{g} = (D \times P_x) / P_y$ ,  $\overline{EF} = A(1 - D/P_y)$ ) and by substituting in Equations (9) and (10) we obtain:

$$\overline{EF} = (H \tan \alpha - R \cos \gamma) / \tan \alpha \tag{24}$$

$$\bar{g} = R \sin \gamma / \tan \alpha \tag{25}$$

and the shaded area is

$$S^{sh} = \overline{EF} \times (L - \bar{g}) \tag{26}$$

where  $0 \leq \overline{EF} \leq A$  and  $0 \leq \bar{g} \leq L$ ;  $\overline{EF} \geq 0$  and  $\bar{g} \geq 0$ ; otherwise  $\overline{EF} = 0$  and  $\bar{g} = 0$  and  $S^{sh} \geq 0$  for non-negative values for both  $\overline{EF}$  and  $\bar{g}$  otherwise  $S^{sh} = 0$ .

For long collectors,  $L \gg H$ , the shaded area is given by  $L(H - x)$  (see Figure 11) where

$$x = k \cos(\gamma_s - \gamma_c) \tag{27}$$

and

$$k = R / \tan \alpha \tag{28}$$

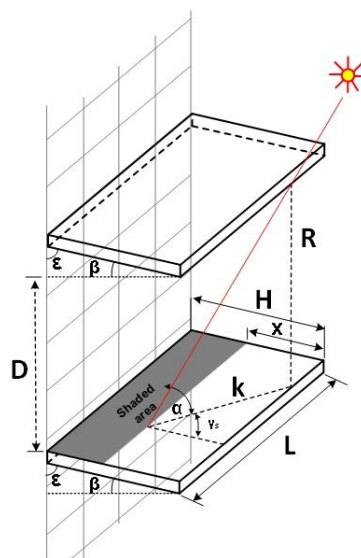


Figure 11. Shaded area on bottom collector.

Substituting Equation (28) in Equation (27) we get:

$$x = R \cos(\gamma_s - \gamma_c) / \tan \alpha \tag{29}$$

and the relative shaded area is given by:

$$S^{sh} = \frac{L(H - x)}{L \times H} = 1 - \frac{R \cos(\gamma_s - \gamma_c)}{H \tan \alpha} \tag{30}$$

The exposed width  $x$  is bounded by the width  $H$  of the collector; see Figure 11, i.e.,  $S^{sh} \geq 0$ .

### 3. Results

#### 3.1. Shaded Area

The relative shaded area, in percentage, on a bottom collector cast by an overhang top collector, horizontally installed, is depicted in Figure 12. The collector is of a long edge  $L$  and a width  $H = 0.941m$ . The figure shows the daily variation of the relative shaded area on April 21st (dotted lines) and on June 21st (solid lines), for three distances  $D = 1.0, 2.0, 3.0m$ . The starting and leaving times of the solar rays on the bottom collector are denoted by  $T_{cr}$  and  $T_{cs}$ , respectively. On April 21st, no shading occurs between about 09:30 and 14:30 on the bottom collector for  $D = 3.0m$ . The shaded area is smaller in winter months.

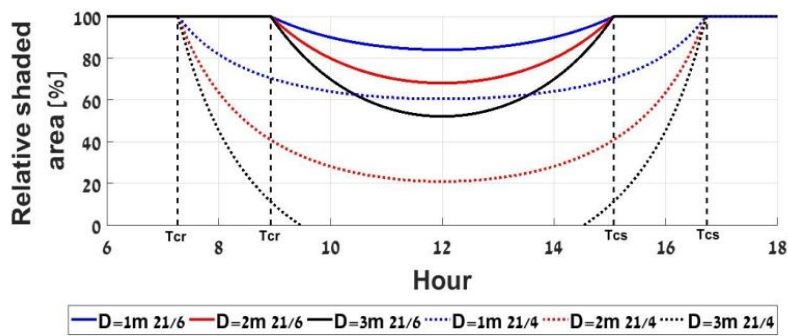


**Figure 12.** Daily variation of percentage shaded area on the bottom collector on April ( . . . ) and June (—) 21st,  $H = 0.941m$ ,  $D = 1.0, 2.0, 3.0m$ .

The relative shaded area, in percentage, on the ground cast by an overhang roof of a carport is depicted in Figure 13. The roof is of a long edge and the overhang width is  $H = 5.0m$ . The figure shows the daily variation of the relative shaded area on April 21st (dotted lines) and on June 21st (solid lines), for two distances  $D = 3.0, 5.0m$ . At noon hours in summer months, the solar rays still penetrate the parking area, and in winter months the parking area enjoys the sun.

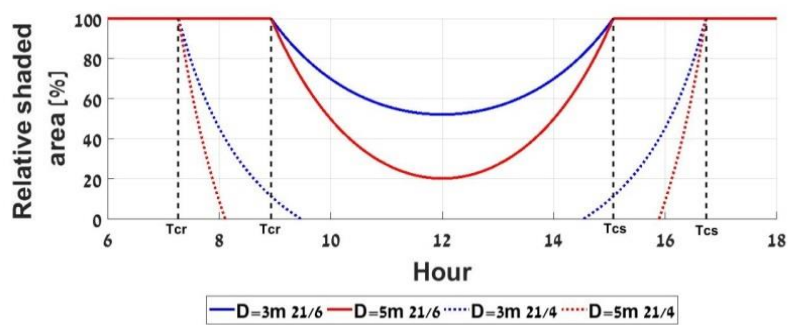


**Figure 13.** Daily variation of percentage shaded area on the ground on April ( . . . ) and June (—) 21st,  $H = 5.0m$ ,  $D = 3.0, 5.0m$ .

### 3.2. Incident Radiation on Overhang PV Collectors

In this section we develop the equations for the incident solar radiation on a single and on multiple overhangs attached to south-facing vertical walls.

#### 3.2.1. Single Overhang Collector

The global solar irradiance  $G_\epsilon$ , in  $(W/m^2)$ , incident on an inclined overhang PV collector with an angle  $\epsilon$  consists of the direct beam  $G_b$ , diffuse irradiance on a horizontal plane  $G_{dh}$ , reflected irradiance from the wall above the overhang, and the sky and wall view factors:

$$G_\epsilon = G_b \cdot \cos \theta + F_{H \rightarrow sky} \cdot G_{dh} + ref_{wall} \cdot F_{H \rightarrow wall} \cdot G_g \tag{31}$$

where  $\theta$  is the angle between the solar beam and the normal to the collector given by [16]:

$$\cos \theta = \cos \beta \sin \alpha + \sin \beta \cos \alpha \cos(\gamma_s - \gamma_c) \tag{32}$$

The angles involved in solar calculation are shown in Figure 14.

$\alpha$  is the sun elevation angle;  $\beta$  is the collector inclination angle with respect to horizontal plane,  $\beta = 90 - \epsilon$  ( $\epsilon$  is the collector angle with respect to the wall) and  $\gamma = \gamma_s - \gamma_c$  is the difference between the sun and collector azimuths with respect to south.  $G_g$  is the global incident irradiance on the wall;

$F_{H \rightarrow sky}$  is the view factor of the surface  $H$  to sky;  $F_{H \rightarrow wall}$  is the view factor of the surface  $H$  to wall;  $ref^{wall}$  is the reflectance of the wall above the collector.

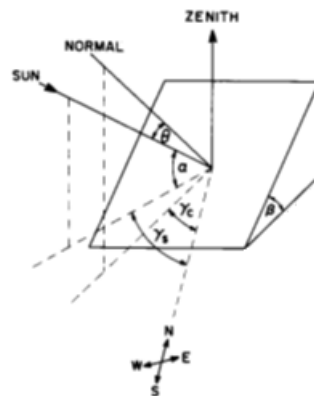


Figure 14. Angles involved in solar radiation calculations.

The collector is open to sky therefore the view factor to sky of a single collector is [17]:

$$F_{H \rightarrow sky} = (1 + \cos \beta) / 2 = (1 + \sin \epsilon) / 2 \tag{33}$$

and view factor of the collector to the wall is given by:

$$F_{H \rightarrow wall} = (1 - \cos \beta) / 2 = (1 - \sin \epsilon) / 2 \tag{34}$$

The reflected irradiance,  $ref^{wall} \cdot F_{H \rightarrow wall} \cdot G_g$ , of the wall on the collector is small with respect to the beam and diffuse irradiance. For  $\epsilon = 60^\circ$ , for example,  $F_{H \rightarrow wall}^f = 0.067$  and multiplying by a high reflectance coefficient of the wall would result only in about 2% of the global irradiance  $G_\epsilon$ .

The yearly direct beam incident irradiation on the top collector,  $q_b^{top}$ , per unit area, is given in Wh/m<sup>2</sup> by:

$$q_b^{top} = \sum_{n=1}^{n=365} \sum_{T_R}^{T_S} G_b \cos \theta \Delta T \tag{35}$$

and the diffuse incident radiation  $q_d^{top}$ , per unit area, in Wh/m<sup>2</sup> is given (see Equation (33)) by:

$$q_d^{top} = \left( \frac{1 + \sin \epsilon}{2} \right) \times \sum_{n=1}^{n=365} \sum_{T_{SR}}^{T_{SS}} G_{dh} \Delta T \tag{36}$$

where  $\Delta T$  is the summation time interval (for solar data sampled every hour  $\Delta T = 1$ ) from sun rise  $T_R$  to sunset  $T_S$  on the collector for the beam irradiance, and from sun rise  $T_{SR}$  to sun set  $T_{SS}$  for the diffuse irradiance. The other summation is from January 1 ( $n = 1$ ) to December 31 ( $n = 365$ ).

### 3.2.2. Multiple Overhang Collectors

In multiple overhang collectors the top collector casts a shadow on the bottom collector forming a shaded area as shown in the Figure 11.

The yearly direct beam incident irradiation on the bottom collector,  $q_b^b$ , per unit area, is given in Wh/m<sup>2</sup> by:

$$q_b^{bot.} = \sum_{n=1}^{n=365} \sum_{T_R}^{T_S} G_b \cos \theta (1 - S^{sh}) \Delta T \tag{37}$$

where  $S^{sh}$  is given by Equation (29).

The yearly diffuse incident irradiation on the bottom collector,  $q_d^{bot.}$ , per unit area, is given in Wh/m<sup>2</sup> by:

$$q_d^{bot.} = F_d^{bot.} \sum_{n=1}^{n=365} \sum_{T_{SR}}^{T_{SS}} G_{dh} \Delta T \tag{38}$$

where the sky view factor  $F_d^{bot.}$  of the bottom collector is calculated based on the ‘‘Crossed-String Method’’ [18], see Figure 15:

$$F_d^b = \frac{AC + BC - AB}{2AC} \tag{39}$$

resulting in:

$$F_d^{bot.} = \frac{H + D + H \cos \epsilon - [D^2 + (H \sin \epsilon)^2]^{1/2}}{2H} \tag{40}$$

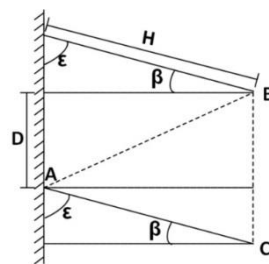


Figure 15. Calculation of sky view factor.

The yearly global incident irradiation on the top and bottom collectors, respectively, in Wh/m<sup>2</sup>, are,

$$q_y^{top} = q_b^{top} + q_d^{top} \tag{41}$$

$$q_y^{bot.} = q_b^{bot.} + q_d^{bot.} \tag{42}$$

Multiplying Equations (41) and (42) by the collector area  $H \times L$  results in the collectors’ yearly incident energies in Wh. Table 1 shows the results of yearly incident energies, in kWh, on the top and bottom PV overhang collectors for three distances  $R = 1.0, 2.0, 3.0\text{ m}$ ,  $H = 0.941\text{ m}$ ,  $L = 30\text{ m}$ ,  $\epsilon = 70^\circ$  ( $\beta = 20^\circ$ ), (see Figure 11 and Equations (35)–(38), (40)–(42)) for Tel Aviv (latitude  $\phi = 32^\circ\text{N}$ ).  $E_{b-top}$ ,  $E_{d-top}$ ,  $E_{g-top}$  are the beam, diffuse and global energy on the top collector, respectively and  $E_{b-bot.}$ ,  $E_{d-bot.}$ ,  $E_{g-bot.}$  are the beam, diffuse and global energy on the bottom collector, respectively. The percent difference in global energy between the top and bottom collectors are 48.87, 32.95, 24.48%, for  $R = 1.0, 2.0, 3.0\text{ m}$ , respectively. This difference stems from shading on the bottom collector and from its lower sky view factor.

Table 1. Annual incident energies on top and bottom PV overhang collectors,  $H = 0.941\text{ m}$ ,  $L = 30\text{ m}$ ,  $\epsilon = 70^\circ$ ; see Figure 11.

$R(m)$ Distance	$E_{b-top}$ (kWh) Beam-top	$E_{d-top}$ (kWh) Diffuse-top	$E_{g-top}$ (kWh) Global-top	$E_{b-bot.}$ (kWh) Beam-bottom	$E_{d-bot.}$ (kWh) Diffuse-bottom	$E_{g-bot.}$ (kWh) Global-bottom
1.0	38,644	15,297	53,941	20,654	6,928	27,582
2.0	38,644	15,297	53,941	27,418	8,750	36,168
3.0	38,644	15,297	53,941	30,805	9,392	40,197

### 3.3. Bifacial PV Modules

Bifacial PV modules have been developed with the purpose of enhancing the power output over conventional (mono-facial) PV modules because bifacial modules can absorb solar radiation from both the front and the rear side. Their applications are useful when the nearby ground or other surfaces are

highly reflective [19–22]. The application and mainly the physics of bifacial cells are presented in the dissertation [19]. A study by simulation and field testing of vertical installed bifacial modules appear in [20]. Reference [21] compares the performance of vertical and south facing bifacial PV collector fields. A recent article [22] on simulating the energy yield of a bifacial photovoltaic plant investigates the influence of ground size, cast ground shadow and ground reflectivity on the energy yield. The only reference, as far as we know, on bifacial PV modules suggested for window shading by overhangs is mentioned in [23]. The overhang uses white semitransparent reflector sheet placed behind the bifacial modules to enhance the reflected radiation on the rear side of the PV module. The present study suggests using bifacial PV modules in its natural manner without providing additional external reflective material, i.e., using the natural reflectance from walls and grounds of the building to assess the additional energy contribution of the rear side of the PV bifacial module.

The global incident irradiance  $G_\varepsilon$ , in  $(W/m^2)$ , on the front side of the PV collector modules inclined by  $\varepsilon$  with respect to a wall is given by [24] (see Figure 16):

$$G_\varepsilon = G_b \cdot \cos \theta + F_{H \rightarrow sky}^f \cdot G_{dh} + ref_{wall}^f \cdot F_{H \rightarrow wall}^f \cdot G_g \tag{43}$$

The global incident irradiance on the rear side of the PV collector modules consists of the irradiance from ground, from shaded wall S and from unshaded wall:

$$G_\varepsilon = al \cdot F_{H \rightarrow grd}^r \cdot G_{dh} + ref_{wall.s} \cdot F_{H \rightarrow wall.s}^r \cdot G_{dh} + ref_{wall.us} \cdot F_{H \rightarrow wall.us}^r \cdot G_g \tag{44}$$

where  $F_{H \rightarrow sky}^f$  is the view factor of front surface H to sky;  $F_{H \rightarrow wall}^f$  is the view factor of the front surface H to wall;  $F_{H \rightarrow grd}^r$  is the view factor of the rear surface H to ground;  $F_{H \rightarrow wall.s}^r$  is the view factor of rear side surface to shaded wall;  $F_{H \rightarrow wall.us}^r$  is the view factor of rear surface H to unshaded wall;  $al$  is the ground albedo;  $ref_{wall}^f$  is the reflectance of the wall above the collector;  $ref_{wall.s}$  is the reflectance of the shaded wall;  $ref_{wall.us}$  is the reflectance of the unshaded wall below the collector.

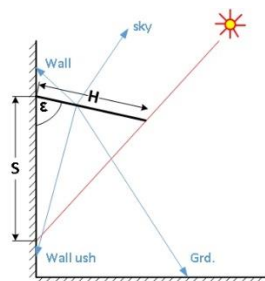


Figure 16. View factor to sky, wall and ground.

The different view factor expressions were developed in [24] and adaptations were made to the configuration in Figure 16. In multiple overhangs, the bottom of the top collector receives also reflected radiation from the top of the bottom collector.

The view factor of the rear-side of the collector to shaded wall is developed in [24] and is:

$$F_{H \rightarrow wall.s}^r = \frac{H + S - [H^2 + S^2 - 2HS \cos \varepsilon]^{1/2}}{2H} \tag{45}$$

Note that the shaded wall S varies with time during the day with the position of the sun, see Figure 5.

The view factor of the rear-side of the collector to unshaded wall is given in [24] and after manipulation we get:

$$F_{H \rightarrow wall.ush}^r = \frac{W_{wall.ush} + [H^2 + S^2 - 2HS \cos \epsilon]^{1/2}}{2H} - \frac{[(S - H \cos \epsilon + W_{wall.ush})^2 + (H \sin \epsilon)^2]^{1/2}}{2H} \quad (46)$$

The view factor between the rear-side of collector to the ground is based on [24] and after manipulation the view factor is:

$$F_{H \rightarrow grd.}^r = \frac{H - S - W_{wall.ush} + [(H \sin \epsilon)^2 + (S - H \cos \epsilon + W_{wall.ush})^2]^{1/2}}{2H} \quad (47)$$

### Bifacial PV Overhang

The contribution of the annual energy on the rear side of the bifacial overhang collector is demonstrated by an example for the following overhang given data:

$$H = 0.941m, L = 30m, S + W_{wall.ush} = 3.0m, \epsilon = 70^\circ, al = 0.1, ref_{wall.s} = 0.1, ref_{wall.ush} = 0.4$$

The rear side annual energy components are (using Equations (44)–(47)): ground reflected energy: 1055 kWh ; shaded wall reflected energy: 684 kWh ; unshaded wall reflected energy: 1281 kWh .

The total annual reflected incident energy on the rear side of the overhang collector amounts to 3020 kWh, comprising 5.6% of the front side overhang energy. Based on the above-mentioned energies one may calculated the energy contribution for different reflectance coefficients of the ground, shaded wall and unshaded wall.

## 4. Discussion

Not much analytical work has been published on the shadow variation on windows, walls and grounds including shaded areas cast by protruding structures such as overhangs. There are many tools available for shading analysis and designing overhang shading structures; however, they do not provide the insight and the mathematical methodology how these tools were derived, what are the assumptions, what was considered and was neglected. The general analytical expressions developed in the present study specify explicitly the various parameters of shading by overhangs and permit the flexibility in parameter variation. Based on the methodology and the expressions, one may extend the study on shadows for different overhang configurations. The novel contribution of the present study includes also the incident radiation on PV overhang collectors, installed one above the other, in the presence of shading. The effect of the sky view factor affecting the diffuse radiation on PV collectors was recently introduced and implemented in the calculation of incident radiation on PV modules on overhangs. A novel application of bifacial PV modules was introduced in the present study including the computation of the energy gain of the rear side of the bifacial PV modules.

## 5. Conclusions

Building integrated photovoltaic structures are playing nowadays an important role in solar electric energy generation. Photovoltaic modules integrated into buildings may provide shading to windows, doors and carports, and, at the same time, generate electrical energy. The study develops basic mathematical expressions, step by step, for shadows cast by overhangs (single and multiple overhangs placed one above the other) and calculates the annual incident energy (beam, diffuse and global energy) on overhangs made up of PV modules. The calculation of the diffuse incident radiation involves the view factors to sky, to ground and between overhangs. The present study suggests using bifacial PV modules for overhangs to increase the PV output power contributed by the reflective energy from walls and ground to the rear side of the bifacial PV module. A power gain of more than 5% was demonstrated. The new approach for analyzing shadows cast by overhangs and the determination

of the incident radiation on PV overhang collectors provides an inside and methodology of shadow analysis on protruding structures in BIPV.

**Author Contributions:** J.A.—conceptualization, writing—original draft preparation; A.A.—software; T.M.—methodology.

**Funding:** This research received no external funding and performed for a degree in engineering.

**Conflicts of Interest:** The authors declare no conflict of interest.

## References

- James, T.; Goodrich, A.; Woodhouse, M.; Margolis, R.; Ong, S. *Building-Integrated Photovoltaics (BIPV) in Residential Sector: An Analysis of Installed Rooftops Systems Prices*; Technical Report NREL/TP-6A20-53103; National Renewable Energy Lab: Golden, CO, USA, 2011.
- Kaan, H.; Reijnga, T. Photovoltaics in an architectural context. *Prog. Photovolt. Res. Appl.* **2004**, *12*, 395–408. [[CrossRef](#)]
- Gaiddon, B.; Kaan, H.; Munro, D. *Photovoltaics in the Urban Environment, Lessons Learned from Large-Scale Projects*; Taylor & Francis Group: London, UK, 2009; ISBN 978-1-84407-771-7.
- Loulas, N.M.; Karteris, M.M.; Pilavachi, P.A.; Papadopoulos, A.M. Photovoltaics in urban environment: A case study for typical apartment buildings in Greece. *Renew. Energy* **2012**, *48*, 453–463. [[CrossRef](#)]
- Sick, F.; Erge, T. *Photovoltaics in Buildings—A Design Handbook for Architects and Engineers*; James & James: London, UK, 1996; ISBN 1-873936-59-1.
- Castellanos, S.; Sutter, D.A.; Kammen, D.M. Rooftop solar photovoltaic potential in cities: How scalable are assessment approaches? *Environ. Res. Lett.* **2017**, *12*, 125005. [[CrossRef](#)]
- Vulkan, A.; Kloog, I.; Dorman, M.; Erell, E. Modeling the potential for PV installation in residential buildings in dense urban areas. *Energy Build.* **2018**, *169*, 97–109. [[CrossRef](#)]
- Kermani, A.Y.; Nasrollahi, F.; Mahdavinjad, M. Investigation of the relationship between depth of overhang and amount of daylight indicators in office buildings of Kerman city. *Environ. Health Eng. Manag. J.* **2018**, *5*, 129–136. [[CrossRef](#)]
- Robbins, C.L. *Daylighting: Design and Analysis*; Van Nostrand Reinhold: New York, NY, USA, 1986.
- Budin, R.; Budin, L. A mathematical model for shading calculation. *Sol. Energy* **1982**, *29*, 339–349. [[CrossRef](#)]
- Yoo, S.H. Simulation for an optimal application of BIPV through parameter variation. *Sol. Energy* **2011**, *85*, 1291–1301. [[CrossRef](#)]
- Jones, R.E., Jr. Effects of overhang shading of windows having arbitrary azimuth. *Sol. Energy* **1980**, *24*, 305–312. [[CrossRef](#)]
- Yolanda, V.; Jones, R.E. Shading effect of finite width overhang on windows facing toward the equator. *Sol. Energy* **1983**, *30*, 171–180.
- Sharp, K. Calculation of monthly average insolation on shaded surface and any tilt and azimuth. *Sol. Energy* **1982**, *28*, 531–538. [[CrossRef](#)]
- Pongpattana, C.; Rakkwamsuk, P. Efficient algorithm and computing tool for shading calculation. *Songklanakarin J. Sci. Technol.* **2006**, *28*, 375–386.
- Bany, J.; Appelbaum, J. The effect of shading on the design of a field of solar collectors. *Sol. Cells* **1987**, *20*, 201–228. [[CrossRef](#)]
- Duffie, J.A.; Beckman, W.A. *Solar Engineering of Thermal Processes*; John Wiley & Sons, Inc.: Hoboken, NJ, USA, 1991.
- Hottel, H.C.; Sarofin, A.F. *Radiative Transfer*; McGraw Hill: New York, NY, USA, 1967; pp. 31–39.
- Duran, C. Bifacial Solar Cells: High Efficiency Design, Characterization, Module and Applications. Ph.D. Thesis, University of Konstanz, Konstanz, Germany, 2012.
- Joge, T.; Eguchi, Y.; Imazu, Y.; Araki, I.; Uematsu, T.; Matsukuma, K. Application and field test of bifacial solar modules. In Proceedings of the 29th IEEE Photovoltaic Specialists Conference, New Orleans, LA, USA, 19–24 May 2002.
- Appelbaum, J. Bifacial photovoltaic panels field. *Renew. Energy* **2016**, *85*, 338–343. [[CrossRef](#)]

22. Chudinow, D.; Haas, J.; Diaz-Ferran, G.; Moreno-Leiva, S.; Eltrop, L. Simulating the energy yield of a bifacial photovoltaic power plant. *Sol. Energy* **2019**, *183*, 812–822. [[CrossRef](#)]
23. Hezel, R. Novel application of bifacial solar cells. *Prog. Photovolt. Res. Appl.* **2003**, *11*, 549–556. [[CrossRef](#)]
24. Appelbaum, J. The role of view factors in solar photovoltaic fields. *Renew. Sustain. Energy Rev.* **2018**, *81*, 161–171. [[CrossRef](#)]



© 2019 by the authors. Licensee MDPI, Basel, Switzerland. This article is an open access article distributed under the terms and conditions of the Creative Commons Attribution (CC BY) license (<http://creativecommons.org/licenses/by/4.0/>).